Biomaterials Science

ROYAL SOCIETY OF CHEMISTRY

PAPER

View Article Online
View Journal | View Issue

Cite this: *Biomater. Sci.*, 2025, **13**, 3585

From saccharides to synthetics: exploring biomaterial scaffolds as cell transduction enhancers†

Micah Mallory,[a,b] Emma Grace Johnson,[a] Soumen Saha,[c] Sanika Pandit,[a,b] Joshua T. McCune,[d] Mengnan Dennis,[b,e] Jessica M. Gluck,[b,e] Craig L. Duvall,[d] Ashley C. Brown,[a,b,f] Ashutosh Chilkoti[c] and Yevgeny Brudno[*a,b,g,h]

Received 28th November 2024,
Accepted 26th April 2025

DOI: 10.1039/d4bm01588f

rsc.li/biomaterials-science

Dry, transduction biomaterial scaffolds (Drydux) represent a novel platform for enhancing viral transduction, achieving drastic improvements in transduction efficiency (from ~10% to >80%) while simplifying production of potent genetically engineered cells. This technology addresses a critical bottleneck in cell therapy manufacturing, where conventional methods require complex protocols and often yield suboptimal results. However, the underlying material science driving Drydux-enhanced transduction remains unclear. Here, we comprehensively assess biomaterial properties that influence viral transduction enhancement through systematic testing of polysaccharides, proteins, elastin-like polypeptides (ELPs), and synthetic polymers. Our findings reveal that surface porosity and liquid absorption are primary drivers of transduction enhancement, while polymer charge and flexibility play secondary roles. Negatively charged and flexible materials—particularly gelatin, hyaluronan, and alginate—demonstrated superior performance. Notably, despite promising material characteristics, synthetic polymers failed to enhance transduction, highlighting the unique advantages of specific biomaterial compositions. By elucidating these structure–function relationships, this work establishes design principles for optimizing biomaterial-enhanced transduction and expands the Drydux platform's potential for transforming cell therapy manufacturing, regenerative medicine, and beyond.

Introduction

Biomaterial scaffolds are a powerful tool for producing transformative genetically engineered cells that can be harnessed as research tools as well as potent therapeutic agents against cancer[1,2] and genetic disorders.[3–5] Genetically engineered cells represent a transformative therapeutic platform, but current approaches remain limited by inefficient viral transduction methods. Current approaches face a critical trade-off: highly efficient methods like spinoculation and microfluidics require cumbersome workflows and specialized equipment while simplified mixing protocols yield poor transduction rates.[6,7]

To address this need for improved virus transduction enhancement, we recently developed Drydux, a biomaterials-driven "dry transduction" platform that achieves both simplicity and efficiency. Drydux dramatically improves transduction rates across multiple cell and virus types,[8–10] leading to their recent commercialization by Takara Bio. These scaffolds show particular promise in chimeric antigen receptor (CAR) T cell manufacturing, where they were incorporated into a one-day, all-in-one, implantable CAR T cell manufacturing and delivery device.[11,12]

Drydux has proven effective as both a reagent and therapeutic device, but the underlying mechanism driving its success remains unclear. Our initial studies identified liquid absorption and macroporosity (80–230 μm pores) as key functional parameters.[8,9] However, since these studies focused on alginate, they explored a limited chemical and materials space. Investigating the transduction potential of materials beyond alginate could help identify chemical properties underpin this new biomaterial phenomenon.

[a]*Joint Department of Biomedical Engineering, University of North Carolina at Chapel Hill and North Carolina State University, Raleigh, NC, USA.*
E-mail: ybrudno@email.unc.edu
[b]*Comparative Medicine Institute, North Carolina State University, Raleigh, NC, USA*
[c]*Department of Biomedical Engineering, Duke University, Durham, NC, USA*
[d]*Department of Biomedical Engineering, Vanderbilt University, Nashville, TN, USA*
[e]*Wilson College of Textiles, North Carolina State University, Raleigh, NC, USA*
[f]*Department of Materials Science and Engineering, Raleigh, NC, USA*
[g]*Department of Pharmacoengineering and Molecular Pharmaceutics, University of North Carolina at Chapel Hill, Chapel Hill, NC, USA*
[h]*Lineberger Comprehensive Cancer Center, University of North Carolina at Chapel Hill, Chapel Hill, NC, USA*

† Electronic supplementary information (ESI) available. See DOI: https://doi.org/10.1039/d4bm01588f

In this report, we systematically investigate how diverse biomaterial properties – including polymer composition, charge, hydrophilicity, and pore structure – influence cell transduction efficiency. By evaluating a broad panel of scaffolds against conventional mixing methods, we aim to uncover the fundamental material science behind Drydux transduction enhancement. Overall, the results strongly support the role charge, polymer strand conformational freedom and liquid absorption in transduction and establish design principles for next-generation biomaterials to accelerate the development and manufacturing of cell-based therapeutics across many disease applications.

Materials and methods

Scaffold synthesis

Saccharides. Alginate scaffolds were prepared as previously reported.[8–10] Briefly, ultrapure alginate (Pronova, MVG) was dissolved in deionized (DI) water for at least one hour before being mixed with an equal volume of 0.4% w/v of calcium-D-gluconate solution for 15 min. The final solution was made to have alginate concentrations that were either 1% w/v or 2% w/v with a calcium concentration of 0.2%. Hyaluronan (LifeCore Biomedical) scaffolds were prepared by dissolving hyaluronan in DI water to create 1% and 2% w/v solutions. Agarose (Millipore Sigma) scaffolds were prepared by heating DI water to 80 °C and then mixing in agarose to create solutions ranging from 0.25–2% w/v. Chitosan scaffolds were made by stirring chitosan (Milipore Sigma) in an 4% acetic acid solution at 80 °C overnight to create solutions with a 1% or 2% w/v concentration. The resulting mixtures were cast in 48-well non-coated tissue culture plates (Corning) at 600 μL per well and frozen at −20 °C overnight. The frozen scaffolds were lyophilized for 72 hours before being removed, packaged with desiccants and stored at 4 °C until used.

Proteins. SpongeCol wafers (Biomatrix) were purchased directly from the manufacturer. Collagen scaffolds were made from Type I bovine collagen solution (Biomatrix, Purcol). 1% w/v scaffolds were directly cast into 48-well non-coated plates while 0.5% solution was achieved by diluting in 1× Dulbecco's phosphate buffer solution (Gibco) before being cast. Gelatin scaffolds were made by dissolving gelatin in DI water, heating to 70 °C to achieve final concentration of 1% or 2% w/v before being sterile filtered (0.22 μm Steriflip) and then cast. Fibrinogen scaffolds were made by diluting human fibrinogen —plasminogen, von Willebrand factor, and fibronectin depleted (Enzyme Research Labs)—with ultrapure water. Fibrin scaffolds were made by combining the human fibrinogen solution, 1× HEPES buffer, and 5 U mL^{-1} of human α-thrombin (Thermo Fisher Scientific) and allowed to polymerize for 2 hours. All protein scaffolds were cast into a 48 well plate at a final volume of 600 μL. The scaffolds were frozen overnight at −20 °C and lyophilized for 72 hours. Dry scaffolds were packaged with desiccants and stored at 4 °C until used.

ELPs. Elastin-like polypeptides (ELPs) were synthesized as previously described.[13–15] Briefly, genes encoding ELP1-5 were synthesized from commercial oligomers (IDT Inc.) and cloned into the pET-24A+ vector. These were recombinantly expressed in BL21(DE3) *E. coli* cells, which were inoculated from frozen DMSO stocks and cultured in TB media with kanamycin (Millipore). Cultures for ELP1-4 were grown for 8 h at 37 °C, while ELP5 cultures were maintained at 25 °C. After induction with 2 mM IPTG (Goldbio), ELP1-4 cultures were grown overnight at 37 °C, and ELP5 at 16 °C. Cells were then pelleted and lysed *via* sonication on ice (3 min: 10 s ON, 40 s OFF) (QSonica, Newtown, CT). Nucleic acids were removed by precipitation with 0.7% w/v aqueous PEI. The supernatant was heated above 55 °C for 10 minutes to induce ELP phase separation, precipitating contaminants. The mixture was then cooled to 4 °C, allowing ELPs to dissolve while leaving contaminants insoluble. The supernatant underwent 2–3 rounds of inverse transition cycling with 3 M NaCl above 55 °C for further purification. Purified ELPs were dialyzed against water for 72 h, lyophilized, and stored with desiccants until scaffold synthesis.

ELP scaffolds were prepared by dissolving the peptides in sterile DI water to the desired concentration, stirring in an ice bath. The solutions were cast in 600 μL volumes in an untreated 48-well plate, frozen at −20 °C, and lyophilized for 72 h. Dry scaffolds were stored at 4 °C with desiccants until use.

Synthetics. Acrylamide scaffolds were made through radical polymerization at low temperatures. Briefly, acrylamide solutions were prepared by dissolving 800 mg of acrylamide and 200 mg of methylenebisacrylamide into DI water for a 5% w/v total monomer concentration. This solution was then degassed and chilled at −20 °C till solution started to freeze. While on ice, 22 mg of ammonium persulfate and 19 μL of tetramethylethylenediamine were then added to a stirring solution and allowed to mix for one minute before being cast into a chilled 48 well plate resting on an ice in ethanol bath. The plate was then moved to −20 °C and left overnight. Polyurethane scaffolds were synthesized as previously describe.[16] Briefly, polyurethane scaffolds were fabricated through a reactive liquid molding process. Briefly, a PEG-based thioketal diol was mixed with a pore opener (calcium stearate), catalyst (TEGOAMIN33), blowing agent (water), and a pore stabilizer (sulfated castor oil) for one minute at 3300 rpm in a Speed Mixer. Lysine triisocyanate was added to this solution, mixed for an additional minute at 3300 rpm, and cured at room temperature overnight. The set polyurethane foams were sectioned into 6 mm scaffolds and washed with ethanol three times to remove unreacted components. The washed scaffolds were vacuum-dried and stored at room temperature until use. Strataprene scaffolds were made *via* a salt fusion technique.[17] Briefly, salt particles were sifted to a size range of 300–400 μm. The salt porogen particles were then lightly compacted and vapor-fused in a cylindrical Teflon mold using humid air as the vapor solvent for the salt particles. Strataprene solutions were prepared by dissolving 20 g of Strataprene pellets in 80 mL of dichloromethane, then carefully dripped onto the fused salt block. Subsequent removal of the fused salt matrix

resulted in a highly interconnected porous foam structure of Strataprene polymer.

Blends. Alginate-acrylamide interpenetrating network scaffolds were made by first dissolving 200 mg of ultrapure alginate, 800 mg of acrylamide and 200 mg of methylenbisacrylamide into 10 mL of ultrapure DI water. Once dissolved, the solution was degassed and chilled till solution started to freeze. While on ice and under nitrogen gas, 10 mL of 0.4% calcium gluconate was added and mixed for 15 minutes to fully incorporate, creating 1% alginate, 0.2% calcium gluconate, and 5% total acrylamide monomers scaffolds. Then ammonium persulfate (22 mg) and tetramethylethylenediamine (19 μL) were added and stirred for one minute. The solution was cast into a chilled 48 well plate resting on an ice in ethanol bath then placed at −20 °C overnight before being lyophilized for 72 hours. Scaffolds were stored at 4 °C with desiccants till used.

Virus production and functional titer

GFP γ-retrovirus was produced using a stably transfected FLYRD118 packaging cell line. Functional titers were determined by transducing 1 million Jurkat cell using Drydux scaffolds in 50 μL dilutions of concentrated virus. Dilutions that result in 10–40% GFP^+ cells were used to calculate the viral functional titer using the following equation and then averaged together: titer (TU mL^{-1}) = (cell number used for infection × percentage of GFP^+ cells)/(virus volume used for infection in each well × dilution fold).

Scanning electron microscopy

All scaffolds were analyzed on a Hitachi SU3900 variable pressure scanning electron microscope. Samples were analyzed at 70 Pa with a nitrogen backfill gas. Images were captured using the ultra-variable detector with a 20 kV accelerating voltage. Assessment of the scaffold porosity was performed on the top surface and was qualitative. Descriptions of alginate pores being well-connected and distributed throughout the surface and body of the scaffold are established by previous literature.[12] SpongeCol also has an established record as a columnar material.[18] Remaining materials surface porosity have been assigned either as being "distributed", "limited", "fiber-like", or "non-porous".

Photographs and absorption rate

All photographs and videos were acquired using a Fujifilm XT-5 mirrorless camera. Videos were acquired at 30 frames per second at 4k resolution at an f10 aperture setting with automatically determined ISO and shutter speed levels. To quantity absorption rate, 50 μL of complete cell culture media was pipetted onto the scaffold and allowed to absorb into the scaffold until fully imbibed or over two hours had elapsed. Absorption rates were quantified through frame-by-frame analysis by calculating the elapsed time between the first droplet contact with the scaffold until the droplet was fully absorbed. All videos were analyzed on the same day and were blindly analyzed a second time on a different day to ensure consistency.

Transduction screening

Transduction enhancement screening was performed using an in house produced γ-retroviral vector encoding for GFP. This screening started by first concentrating the GFP retroviral containing supernatant to 2 million transducing units per 50 μL using Amicon centrifugation filters (MWCO 100 kDa, Millipore) at 1500 g in a swinging bucket rotor. 50 μL of this concentrated supernatant was then used to re-suspend a prepared cell pellet containing 1 million Jurkat cells. This cell and virus suspension was then added directly to each scaffold in 24 well plate or directly onto the culture plate (no scaffold control) using a pipette. A no virus control was prepared by re-suspending 1 million Jurkat cells in 50 μL of complete media only and added directly to the plate. The cell-virus suspension was allowed to incubate for at least 20 minutes before 1 mL of complete cell culture media (RPMI 1640 with L-glutamine (Gibco), supplemented with 10% w/v of fetal bovine serum (Corning) and 100 U mL^{-1} penicillin (Gibco), and 100 μg mL^{-1} streptomycin (Gibco)) was added to each well. After 72 hours, cells were isolated from each scaffold by washing excessively with DPBS. Agarose, collagen, fibrinogen, and synthetic scaffolds required mechanical dissociation in a 40 μm cell strainer—leading to slightly lower cell recovery. All other scaffolds were dissolved through hydration, resulting in near-complete cell recovery. The cells from the scaffold were combined with any cells in the culture media, washed twice with DPBS, stained with anti-human anti-CD3 antibody (BD Biosciences, APC-Cy7) and live/dead stain (Sytox AADvanced, Fisher Scientific) according to manufacturer's protocol, filtered and prepared for flow cytometry.

Flow cytometry

All samples were analyzed on Beckman Coulter Cytoflex with a minimum of 5000 $CD3^+$ events acquired per sample. All events were gated on Jurkat cells by FSC, FSC singlets, viable cells, $CD3^+$, and then GFP^+ (ESI Fig. 6†). Fluorescent intensity data was analyzed on the final GFP^+ population. Analysis of data was performed using FlowJo.

Statistical analysis

All statistical analysis was performed using GraphPad Prism. A one-way ANOVA with Dunnett's multiple comparisons referenced to the no scaffold control was performed unless otherwise noted. A p-value < 0.05 as compared to no scaffold control was taken as significant and denoted with *.

Results

Surface porosity predicts saccharide scaffold transduction enhancement

Polysaccharides are commonly used in the biomaterials field due to their biocompatibility and diverse applications in regenerative medicine, drug and cellular delivery, 3-D cell culture, and wound healing. Among these, alginate,[8,12,19–21] hyaluronan,[22–24] chitosan,[25–28] and agarose[29–31] are some of

the most common materials, many of which have been used in clinical products.[32] Our previous work with Drydux centered on calcium-crosslinked alginate scaffolds. Here, we explored whether other polysaccharide scaffolds would similarly facilitate transduction. Cryogel scaffolds of each polymer were produced through freezing 1% and 2% weight-to-volume (w/v) polymer solutions and lyophilizing the frozen mixtures. All the tested polymers were successfully fabricated into dry scaffolds (Fig. 1A). Scanning electron microscopy (SEM) of the scaffold surfaces revealed diverse pore structures (Fig. 1B). Alginate and hyaluronan scaffolds had a distributed surface porosity with thin dividing walls. Agarose (1% and 2%), on the other hand, had no surface porosity. Interestingly, this non-porous surface obscured an internal porous structure that was arranged in channels within the scaffold (ESI Fig. 1 and 2†). SEM of chitosan revealed a limited surface porosity with distinct, isolated pores surrounded by thick, non-porous walls (Fig. 1B).

Observations of a 50 μL liquid droplet absorbing into the scaffolds revealed strikingly different behaviors (ESI Videos 1–8† and Fig. 1C) between the tested cryogels. On the 1% alginate, the liquid droplet initially sat on top of the scaffold and slowly absorbed into the scaffold over the course of ~9 min (~5.5 μL min^{-1}). The scaffolds remained intact and only slightly constricted in response to the entering liquid droplet. The 2% alginate absorbed all the liquid within three minutes (~20 μL min^{-1}) and slightly collapsed at the location of the droplet over the course of ~15 min. The agarose scaffolds had markedly higher absorption rates (~700 μL min^{-1}) with the 2% scaffold maintaining its shape and the 1% scaffold experiencing ~50% constriction over the course of 1 min. In sharp contrast, the hyaluronan scaffolds fully dissolved over the course of approximately 3 min with the initial absorption completing within ~20 s (~300 μL min^{-1}). The 1% chitosan scaffolds had the fastest absorption rates at ~3000 μL min^{-1} and constricted to roughly one-third of their original size over the course of 1 min. 2% chitosan scaffolds had an absorption rate of ~150 μL min^{-1} and constricted by roughly 50%.

To test transduction enhancement with these scaffolds (Fig. 1D), Jurkat cells (1 million) were mixed with GFP-encoding γ-retrovirus (2 million transducing units) in 50 μL of media and pipetted onto each scaffold. For negative controls, the same solution was pipetted directly onto a culture plate without a scaffold. 2% chitosan scaffolds were excluded from the analysis due to low cell recovery and low cell viability. All

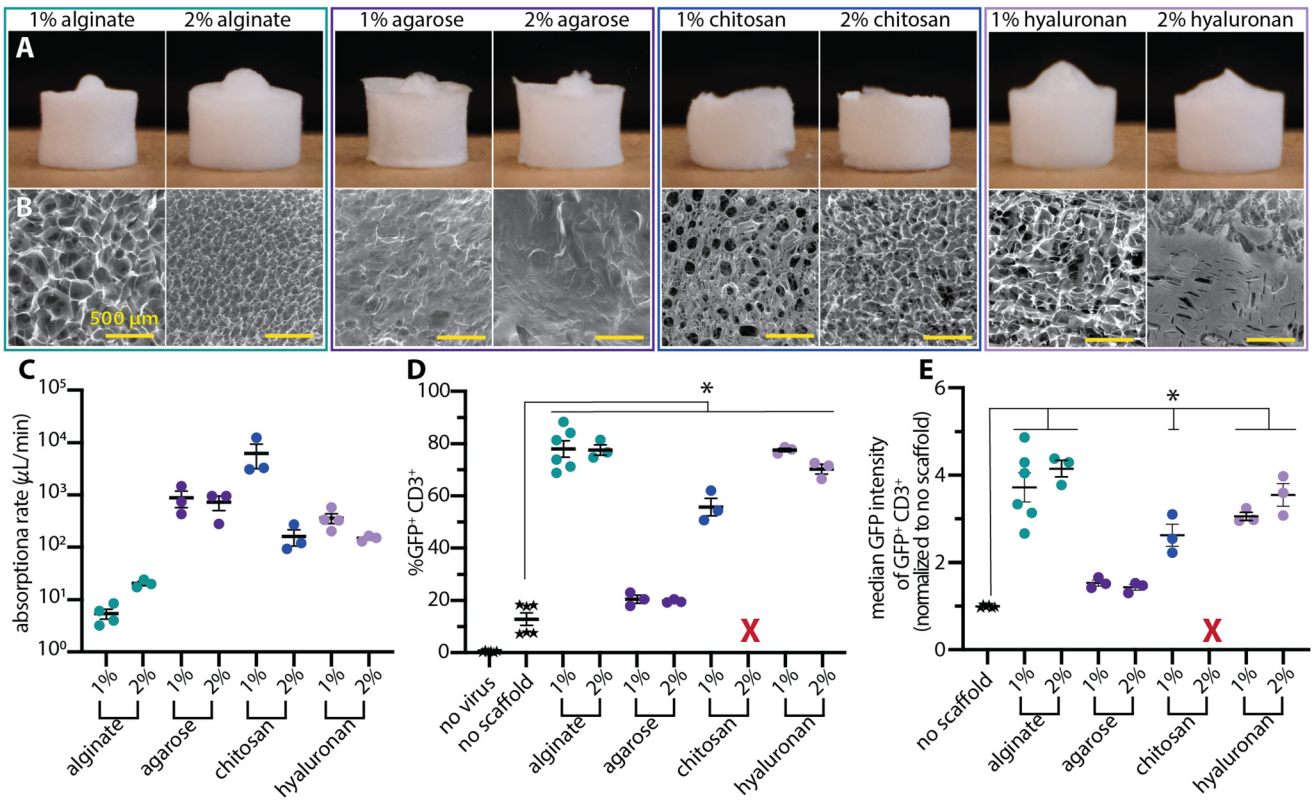

Fig. 1 Saccharide scaffolds mediate viral transduction. Representative (A) photographs of the whole scaffold and scanning electron microscopy (SEM) images of each scaffold's surface (B), highlighting the diverse microstructures that give rise to overall similar macroscale scaffolds. The bumps on the tops of select scaffolds are artifacts of the freezing process and do not impact scaffold behavior. (C) All the absorption rates were above 5 μL min^{-1} but ranged across four orders of magnitude. (D) All teseted scaffolds improved transduction efficiency over mixing the virus and cells together without a scaffold. 2% chitosan was excluded due to low cell recovery and high levels of cytotoxicity (X). (E) Median fluorescent intensity data of the GFP^+ $CD3^+$ subset of cells. All data was analyzed with a one-way ANOVA with Dunnett's multiple comparisons test. A p-value < 0.05 as compared to no scaffold control is denoted by *.

the scaffolds facilitated improved transduction compared to the no scaffold control ($p < 0.05$). However, there was a range of transduction enhancing capabilities with the transduction results closely following the surface characteristics observed in the SEM. The scaffolds with distributed surface porosity (alginate and hyaluronan) resulted in the highest transduction (~78%) while the limited surface porosity of 1% chitosan resulted in slightly decreased transduction enhancement (~56%) and the non-porous surfaces of the agarose scaffolds resulted in the lowest transduction enhancement (~20%).

There was no clear relationship between polymer concentration and transduction results. In all cases, the transduction enhancement of the 1% and 2% concentrations of each material were similar despite differences in observed structural and absorption characteristics.

Protein expression within the transduced population is an alternative readout of the extent of each material's transduction enhancement (Fig. 1E). Hyaluronan-seeded cells had a fluorescence intensity similar to cells from alginate samples, mirroring their similar overall transduction efficiencies (Fig. 1D). Interestingly, 1% chitosan and 1% hyaluronan-treated cells had similar intensity values despite their 20-percentage point difference in transduction efficiency. These results indicates that a material's enhancement of the percent of cells that are transduced could be decoupled from the amount of virus particles transducing individual cells as measured by the MFI of GFP$^+$ cells. This observation may prove useful for achieving further improvements in transduction percentages while modulating the vector copy number in transduced cells.

Protein scaffold concentration modulates transduction

Protein-based scaffolds are a common alternative biomaterial with wide utility in tissue engineering and regenerative medicine.[33–40] We tested a panel of protein-based scaffolds (Fig. 2A) for absorption and transduction. SEM imaging (Fig. 2B) revealed that the gelatin and 1% collagen scaffolds had distributed surface porosity with thin walls. The commercially available collagen-based SpongeCol scaffolds were thinner (1 mm total height) compared to the other scaffolds (4–6 mm total height) and had larger (~500 μm), column-like pores. The fibrinogen and 0.5% fibrin scaffolds had a fiber-like surface appearance interspersed with large void areas rather than true distributed pores. The 2% fibrin scaffolds had distributed, small surface pores (<20 μm).

The protein scaffolds exhibited a wide range of absorption speeds and behaviors with the higher concentration scaffolds consistently requiring more time for absorption (Fig. 2C and

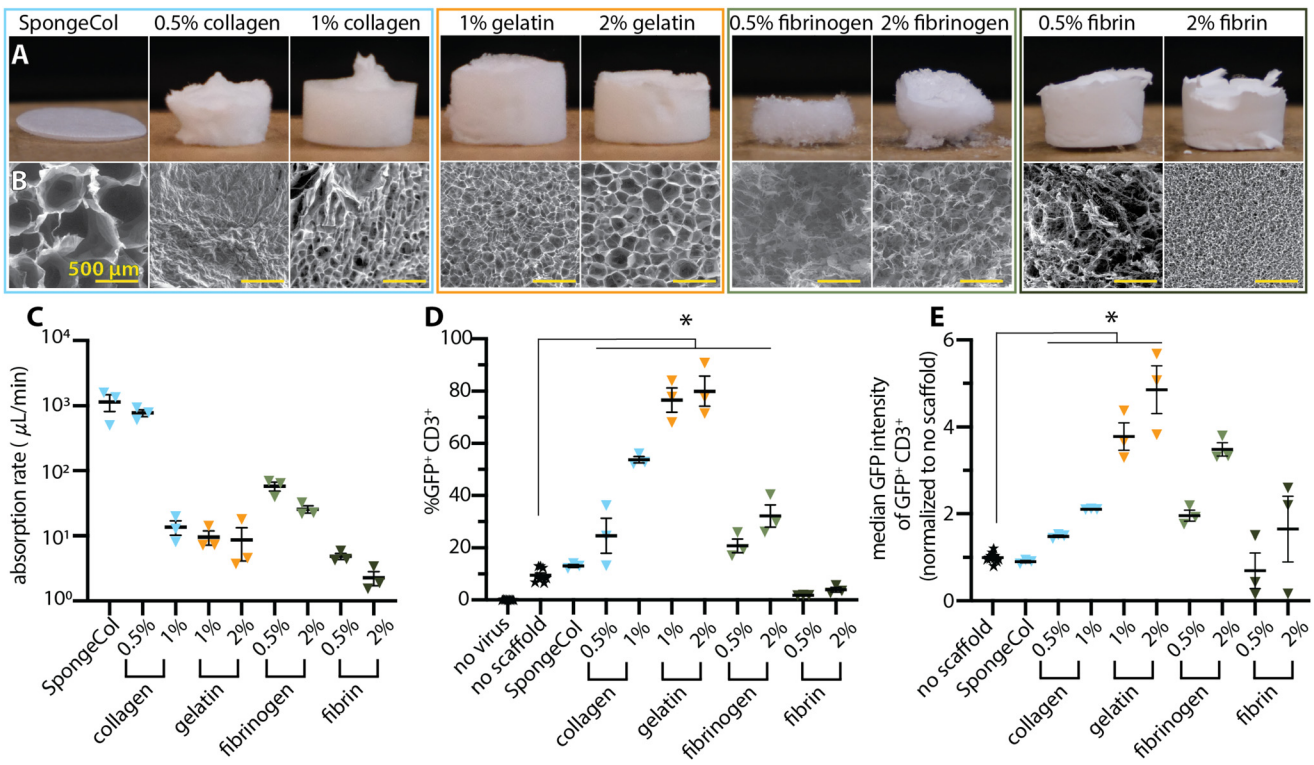

Fig. 2 Gelatin scaffolds mediated transduction more efficiently than other protein scaffolds. Representative photographs of the dry scaffolds (A) and SEM (B) highlight the differences in microscale structure that creates similar macroscale scaffolds. Imperfections in photographed scaffolds are due to the removal process from the plate for photography and were not present in scaffolds evaluated for transduction enhancement. (C) Absorption rates for the protein scaffolds occupied a wide range with outliers on both the high and low end. (D) The transduction efficiencies highlight the dramatic difference between the scaffolds of various materials. (E) Fluorescence median intensity data of the GFP$^+$ CD3$^+$ cell population reveals clear differences between the scaffolds. All data was analyzed with a one-way ANOVA with Dunnett's multiple comparisons. A p-value < 0.05 as compared to no scaffold control is denoted with *.

ESI Videos 9–17†). The collagen-based scaffolds absorbed the liquid fastest with commercially available SpongeCol having the highest absorption rate followed by 0.5% and then 1% collagen scaffolds. These collagen scaffolds generally constricted between 30% and 50% of the initial scaffold size. The 0.5% fibrinogen scaffolds were completely dissolved by the liquid within approximately 5 min, while only the middle portion the 2% fibrinogen scaffolds were dissolved leaving a bowl-like structure remaining. The gelatin scaffolds—both 1% and 2%—had a ~9 μL min^{-1} absorption rate (requiring roughly 6 min to absorb) and maintained their macrostructure with minimal constriction. The 0.5% and 2% fibrin scaffolds required ~12 min and over 30 min, respectively, to absorb the droplet, resulting in the slowest observed absorption rates (~4.5 and ~1.5 μL min^{-1}).

We next tested these scaffolds for their ability to facilitate cell transduction (Fig. 2D). Only a subset of protein scaffolds—collagen, gelatin, and fibrinogen—significantly enhanced cell transduction compared to the no scaffold control. Of these, 1% and 2% gelatin scaffolds mediated the highest transduction, with over an 8-fold increase over the no scaffolds control. 1% collagen had the next highest transduction enhancement with a 5.7-fold increase over the no scaffold control. Interestingly, all the in-house synthesized collagen scaffolds outperformed the commercially available SpongeCol, potentially due to the differences in thickness and pore structure.

In all the tested cases in which a protein scaffold mediated transduction, the higher concentration outperformed the lower concentration. For instance, doubling the collagen concentration resulted in an approximate doubling of the transduction efficiency while for the fibrinogen a 4-fold increase in concentration resulted in 1.5-fold increase in transduction. The gelatin scaffolds also followed this trend with the 2% scaffold slightly outperforming the 1% scaffold. However, since both scaffolds already facilitated high levels of transduction, the observed difference between 1% and 2% gelatin is not statistically significant.

Looking at median fluorescence signal among the transduced cells, several interesting effects were noted (Fig. 2E). In the case of gelatin, the differences between the 1% and 2% scaffolds were more pronounced. Surprisingly, despite 1% gelatin producing a higher percentage of transduced cells than 2% fibrinogen, the two materials had virtually identical fluorescence intensities of their respective transduced cells. Moreover, the 2% fibrinogen scaffolds had double the fluorescence intensity of 1% collagen, despite having half of its transduction efficiency.

ELP scaffold transduction is construct dependent

We next investigated Elastin-like polypeptides (ELPs), whose unique phase transition has attracted significant attention in the biomaterial world for a variety of applications.[41,42] ELPs offer the ability to control the material properties such as hydrophobicity, charge, stereochemistry, and molecular weight through genetic encoding[41] with precise control that is often not possible with synthetic materials. These qualities make ELPs intriguing materials that may help in understanding materials-driven transduction. ELPs of various constructs (Fig. 3A) were processed into dry scaffolds through cryogelation and lyophilization (Fig. 3B). Scaffolds' surfaces were characterized by SEM imaging (Fig. 3C). We identified these constructs based on their wide hydrophobic score and native charge—negative to neutral to positive.

Despite having similar macrostructures in scaffold form, the ELP scaffolds had dramatically different surface morphologies. ELP-5 had distributed surface pores that resemble a honeycomb while the remaining constructs had fiber-like surface appearances. ELP-3 and 4 both had limited to no surface porosity while ELP-2 had fiber-like regions interspersed with non-porous regions. ELP-1 had a fiber-like surface that resembled a web rather than pores, creating an accessible network from the top surface.

ELP scaffolds showed broadly similar liquid absorption rates, despite their varied surface structures (Fig. 3D and ESI Videos 18–22†). ELPs 1–4 absorbed the droplet in <10 s (>300 μL min^{-1}) and completely dissolved into the droplet in 1 min. ELP-5 showed similar behavior, but on a slightly longer timescale, with initial absorption occurring over ~30 s and full dissolution over 2 min.

With the exception of ELP-5, ELP constructs significantly enhanced cell transduction (Fig. 3E). ELP-1 had the highest transduction (~72%). ELP-5 failed to enhance transduction above the no scaffold control despite being the only construct having distributed pores across its surface. In the fluorescence intensity data, ELP-1 again resulted in the greatest difference compared to the no scaffold group (Fig. 3F). Interestingly, despite ELPs-2–4 significantly enhancing transduction over the no scaffold control, their fluorescence intensities were not significantly different than the no scaffold control.

To confirm that the seen effects were not due to the specific polymer concentration, the experiment was repeated with 0.25% w/v polymer solutions and revealed the same trends, albeit with lower overall transduction (ESI Fig. 2†).

Covalent, synthetic polymers fail to mediate transduction

Synthetic polymers are another large class of materials with longstanding use in tissue regeneration and clinical use.[43–48] We synthesized dry, porous scaffolds from acrylamide, polyurethane, and Strataprene—a linear polyester copolymer (Fig. 4A). The SEM surface morphology assessment (Fig. 4B) reveled strikingly different surface topologies than other evaluated material. Acrylamide and Strataprene had more limited surface porosity characterized by an irregular, undulating surface with void areas/crevices interspersed rather than distinct pores. Polyurethane scaffolds had distributed surface pores that were larger and more basin-like.

Absorption properties (Fig. 4C and ESI Videos 23–25†) for the various synthetic materials varied widely. At the extremes, acrylamide absorbed the entire 50 μL droplet in under 1 s (>3000 μL min^{-1}) and constricted to ~10% its original size within ~20 s while the polyurethane scaffolds did not absorb any liquid over the course of a 2 h incubation time. The

A Type	Sequence	Charge/Chain
ELP-1	$(VPGXG)_{120}$ X = A:V 1:4	Neutral
ELP-2	$SKGPG(VPGAG)_{160}(YG)_6$	+1
ELP-3	$SKGPG(VPGAG)_{160}(YG)_6GKGH_8$	+10
ELP-4	$SKGPG(VPGAG)_{160}(YG)_6GKGD_8$	-6
ELP-5	$M\text{-}[9G[V4/A1]GVP)_{15}GD(A)_{25}K]4\text{-}GW$	Neutral

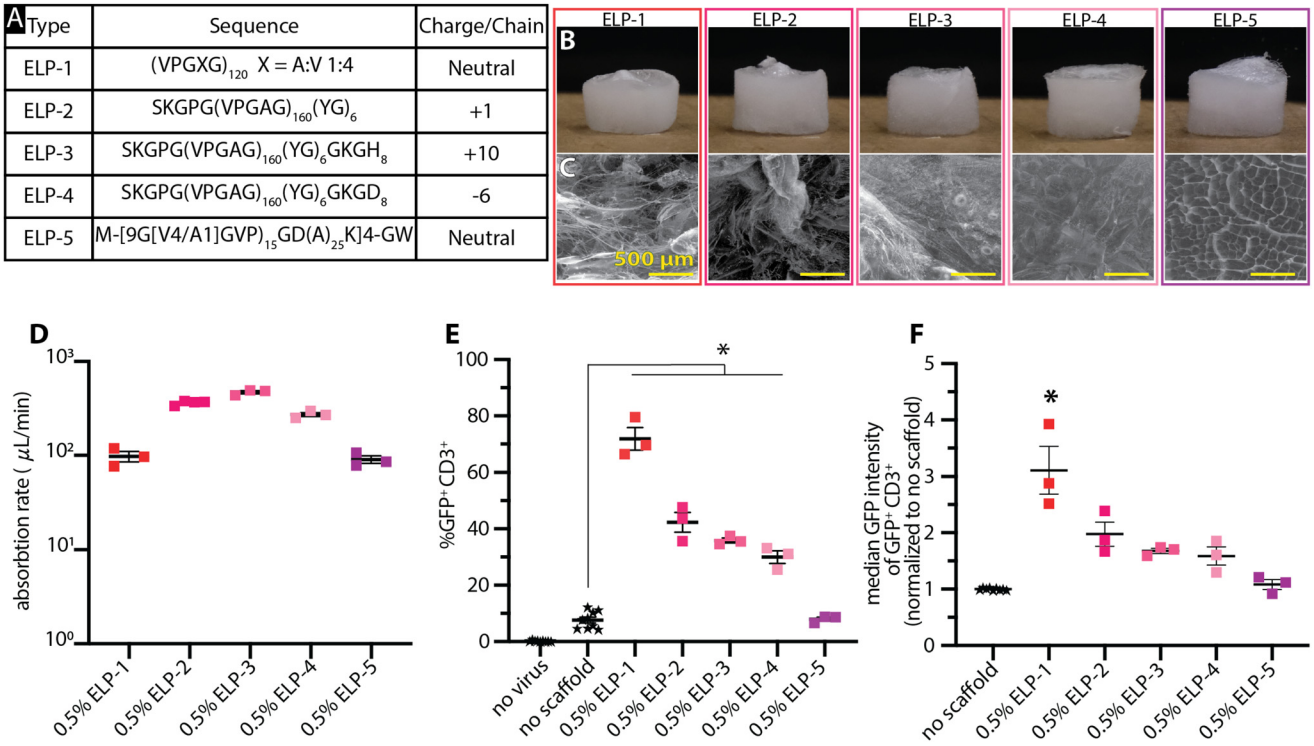

Fig. 3 Elastin like polypeptide (ELP) scaffolds exhibit construct-dependent transduction potentials. (A) Table highlighting the amino acid variation in the ELP constructs and their respective charge per chain ratio. Representative photographs (B) and SEM images (C) highlight the internal structural differences amongst the individual ELP constructs as well as the similarities in their overall scaffold structure. (D) The absorption rates were broadly similar with ELPs-1 and 5 being the slowest. (E) The transduction efficiencies of the scaffolds, highlighting the range of enhancement effect the ELP scaffolds. (F) Median fluorescence intensity from among the GFP^+ $CD3^+$ cells reveal overall lower fluorescence in the cells. All data was analyzed with a one-way ANOVA with Dunnett's multiple comparisons. A p-value < 0.05 is denoted with *.

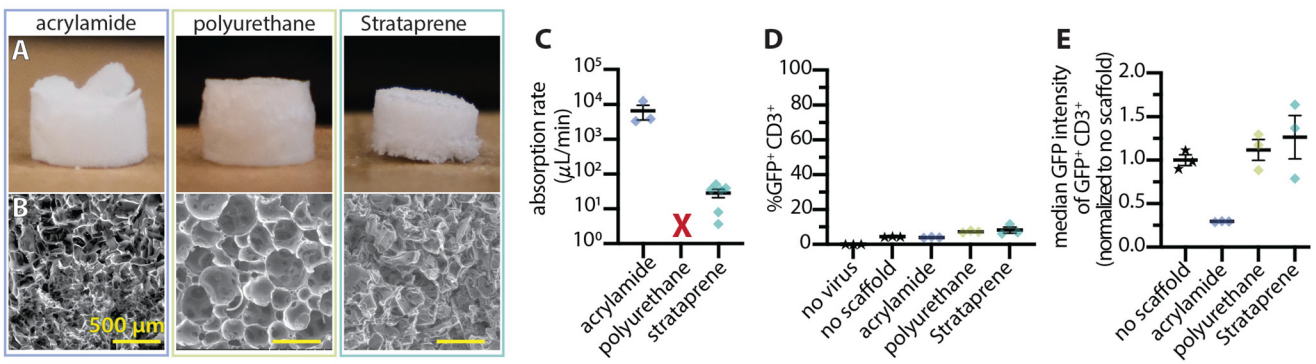

Fig. 4 Synthetic scaffolds fail to mediate transduction. Representative photographs (A) and (B) SEM images showing scaffold surface structure. (C) The absorption rates were highly variable with polyurethane not absorbing any liquid (red X). The transduction efficiency (D) and fluorescent intensity (E) data highlighted that these scaffolds failed to enhance transduction.

Strataprene had an intermediate absorption rate (~40 µL min^{-1}) and did not physically change or mechanically respond during the absorption process.

All the synthetic scaffolds failed to enhance transduction (Fig. 4D). Fluorescent intensity data (Fig. 4E) underscored this point. Interestingly, GFP^+ cells from the acrylamide scaffold group had lower GFP intensity. The poor performance of acrylamide was initially attributed to low cell viability inside the scaffolds (ESI Fig. 3A†). In order to explore if acrylamide's poor performance could be rescued, alginate and acrylamide were combined into an interpenetrating network scaffold. These interpenetrating scaffold maintained cell viability, but still failed to enhance transduction (ESI Fig. 3B and C†).

Combined assessment of all material types

Grouping all the tested materials together by type revealed the material-dependent nature of transduction enhancement. For example, despite each tested saccharide increasing transduc-

tion, these materials differed greatly in the magnitude of that increase—ranging from a ~2-fold increase in transduction efficiency for agarose to a nearly 10-fold increase in the case of alginate and hyaluronan compared to the no scaffold control (Fig. 5A). Overall, 17 of the 24 tested scaffolds (representing 11 of 18 unique materials/constructs) mediated transduction significantly better than the no scaffold control. 9 of those successful 17 scaffolds (representing six unique materials) resulted in transduction efficiencies >50%. 7 of those 9 (four unique materials) had efficiencies >70%. These scaffolds are only a representative subset of each class of material and each concentration of the selected materials.

Analysis of the top six performing constructs (representing 4 distinct materials) reveals several key structural and chemical properties that facilitate optimal viral transduction (Table 1). Alginate, hyaluronan, and gelatin consistently achieved transduction efficiencies above 75%, significantly outperforming other materials tested. These high-performing materials share several characteristics: a highly distributed porous network with thin walls, liquid absorption rates above 5 μL min^{-1}, and negatively charge side chains. Notably, while all top performers exhibited adequate absorption rates, their structural responses to liquid varied considerably—from complete dissolution (hyaluronan) to partial dissolution (gelatin) to minimal constriction (alginate). This variation suggests that initial porosity may be more critical than maintaining scaffold integrity over time. The exceptional performance of ELP-1, despite its neutral charge, indicates that a web-like fibrous structure can compensate for the absence of negative charge when combined with rapid absorption. This analysis supports our hypothesis that optimal transduction enhancement requires a combination of surface porosity, absorption capacity, and preferentially negative polymer charge, while demonstrating that polymer strand conformational freedom and dissolution characteristics likely play secondary roles in the transduction mechanism.

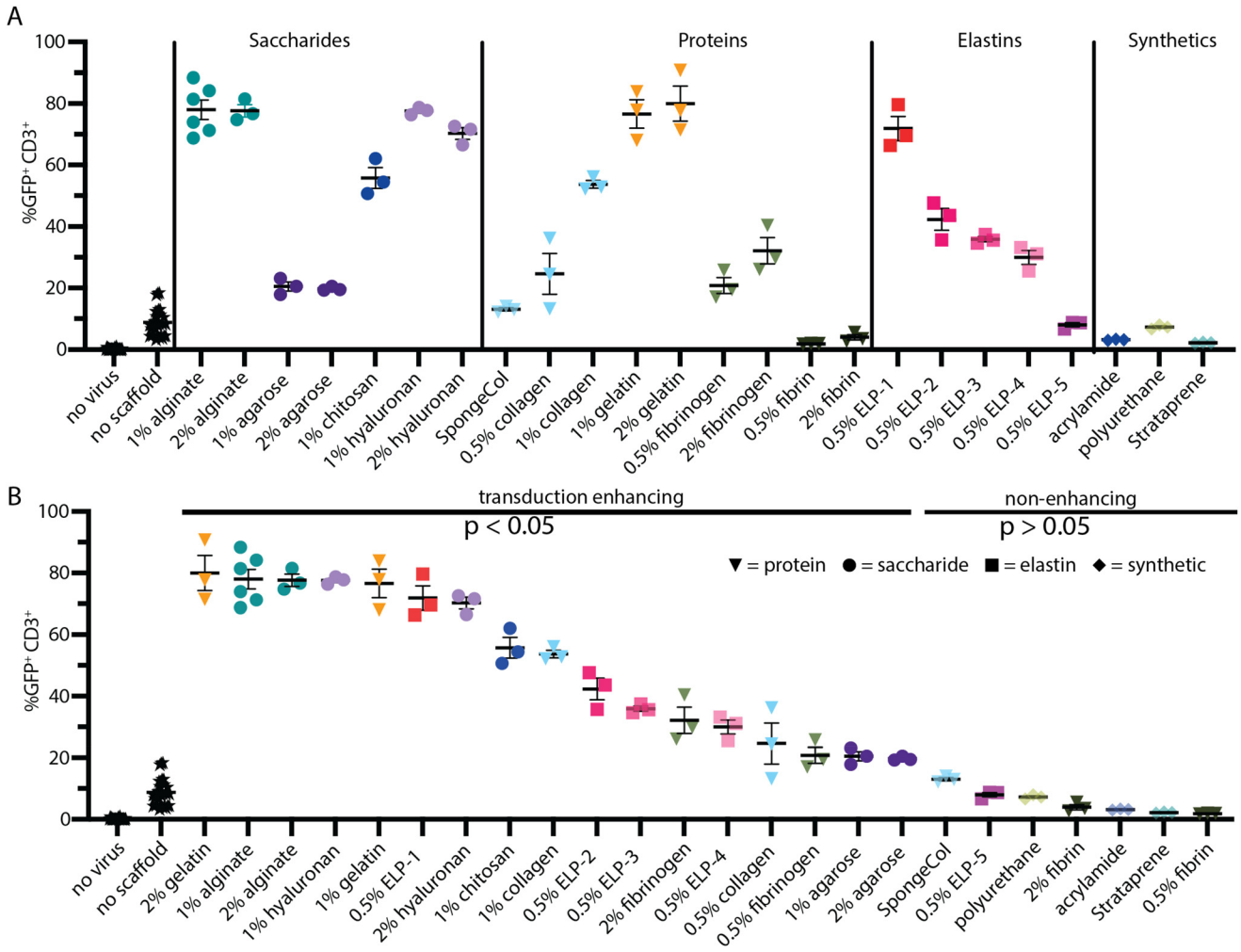

Fig. 5 Materials mediated transduction is neither universal to dry scaffolds nor specific to alginate cryogels. (A) Grouping all materials in a single graph by material class enable quick comparison of transduction promotion behavior. (B) Order ranking the materials highlights that alginate, hyaluronan, and gelatin are the highest performing materials. Data points from the same material regardless of concentration have the same color for easy comparison. Bars show statistical significance ($p < 0.05$) by one-way ANOVA with Dunnett's multiple comparisons relative to no scaffold control.

Table 1 Comparison of top six performing material scaffolds. The top six performing constructs represents four distinct materials. Notably five of the top six have are negative polymers

Material	Transduction efficiency	Absorption rate (μL min^{-1})	Crosslink	Structure after absorption	Structure after 72 hours	Surface topology	Charge
1% alginate	78%	5.4	Ionic	Intact	Intact	Distributed pores	Negative
2% alginate	77.6%	20.6	Ionic	Intact	Intact	Distributed pores	Negative
1% gelatin	76.6%	9.6	Physical	<50% dissolved	Dissolved	Distributed pores	Negative
2% gelatin	80.0%	8.7	Physical	<50% dissolved	Dissolved	Distributed pores	Negative
1% hyaluronan	77.6%	361.2	Physical	Dissolved	Dissolved	Distributed pores	Negative
2% hyaluronan	70.2%	149.2	Physical	Dissolved	Dissolved	Distributed pores	Negative
ELP-1	71.8%	97.6	Physical	Dissolved	Dissolved	Fiber-like	Neutral

To assess the translatability of these findings to clinically relevant primary cells, we tested a subset of materials with donor derived human peripheral blood mononuclear cells (hPBMCs) under identical conditions used with the Jurkat cells (ESI Fig. 5†). As evidenced by the decreased transduction efficiency in all groups, hPBMCs are more recalcitrant to transduction than Jurkats. Overall, however, the transduction enhancement trends for hPBMCs mirrors those of Jurkats. High-performing materials (alginate, hyaluronan) and low-performing materials (fibrin) with Jurkats maintain their relative positions with hPBMCs. Interestingly, we do observe some cell-specific differences, particularly with gelatin scaffolds showing enhanced relative performance with hPBMCs. This divergence likely reflects the inherently different transduction barriers in primary cells compared to immortalized lines. These findings highlight that material selection becomes even more critical when working with clinically relevant primary cells. This initial panel with Jurkat cells narrows the focus to select materials that can then be investigated for use with clinically relevant cell types.

Discussion

We assessed the ability of a variety of dry, macroporous material types to mediate Drydux cellular transduction. We produced representative cryogels from multiple biomaterial classes—polysaccharides, proteins, peptides, and synthetics—and found materials that highly facilitate transduction as well as those that completely fail to enhance transduction. Our findings confirm the importance of porosity for transduction and suggest specific contributions from surface and bulk porosity. In addition, this work supports previous findings that liquid imbibition is paramount to transduction success. While these results complement our previous findings on the importance of porosity, hygroscopy, and absorption, they also demonstrate that these qualities alone are not sufficient to explain material enhanced transduction. Our results for the first time suggest an important role for other inherent material properties, including charge. Surprisingly, synthetic materials seemingly all failed to mediate transduction, even when blended with other successful materials.

This study utilized a γ-retroviral vector to assess transduction efficiency. Viral vectors are particularly relevant as all currently FDA-approved CAR-T cell therapies employee a viral vector to deliver the genetic cargo of interest. Future work could focus on expanding the Drydux phenomenon to nanoparticle systems.

A comprehensive analysis of our current results underscores the importance of porosity while highlighting its inability to fully explain materials-driven transduction. In previous publications with calcium-crosslinked alginate, we reported that surface porosities ranging from 50–230 μm resulted in roughly uniform transduction enhancement[9] while nanoscale porosity failed to enhance transduction.[8] Furthermore, this previous work highlights the importance of constriction points in transduction enhancement.[9] Distributed pores provide a greater number of pathways and constriction points, enabling higher cell/virus collision frequencies. We propose, however, that columnar pores do not have the constricted interconnections that effectively promote cells and virus interactions to drive transduction. In this report, saccharides and protein scaffolds followed a trend with distributed surface porosity (*e.g.* alginate, gelatin, hyaluronan) enhancing transduction while oversized/columnar (SpongeCol), and limited (agarose and 0.5% collagen) surface porosity provided limited transduction enhancement. The fiber-like networks in ELP-1–4 still facilitated transduction with the limited surface porosity in ELP-2–4, potentially accounting for their drop in performance. These results are in line with previous reports 9 that showed decrease of ~10 percentage points in transduction efficiency when alginate lost its surface porosity but maintained its internal porosity. However, it should be noted that distributed porosity does not guarantee successful transduction enhancement. ELP-5, acrylamide, and Strataprene, failed to facilitate transduction despite significant surface porosity. In the future, a fuller investigation into porosity modes (random v. columnar v. fibers) as well as pore size and distribution could shed further light on Drydux transduction enhancement.

The data reveals that the Drydux transduction enhancement fundamentally requires absorption into the scaffold. The absorption rate into the scaffold is related to the hydrophilic properties of the scaffolds as well as its porosity. Across materials, the absorption rate is neither necessarily indicative nor predictive of a scaffold's transduction enhancement capabilities (ESI Fig. 4†). Prior work reported a positive correlation between absorption rate of the cell and virus suspension and transduction enhancement in alginate scaffolds with rates

greater than 5 μL min^{-1} resulting in maximum enhancement.[9] This overall trend was supported by this report as all successful scaffolds absorbed at a rate above 5.5 μL min^{-1}. Alginate, surprisingly, was one of the slowest absorbing successful material (Fig. 1C and ESI Fig. 4†). However, the successful scaffolds had a wide range of rates from 5.5 μL min^{-1} to over 3000 μL min^{-1} with no clear correlation with transduction enhancement across different materials. While the failure of some materials, including polyurethanes and 2% fibrin, may be explained by non-existent or slow absorption, to our surprise, SpongeCol failed to meaningfully enhance transduction despite having a high absorption rate. While the failure of some materials, including polyurethanes and 2% fibrin, may be explained by slow absorption, to our surprise, SpongeCol failed to meaningfully enhance transduction despite having a high absorption rate. We attribute this failure to SpongeCol's thinness. In addition, SpongeCol presents columnar pores,[18] which lack constricting pore interconnections, which we have previously tied to transduction enhancement.[9] We suggest that SpongeCol's shallow, large pores likely mimic standard plate-based mixing, explaining the limited transduction enhancement. Taken together with 2% fibrin's small pores and slow absorption rate, these observations highlight a critical interplay between pore size and absorption: pores that are too small prevent liquid absorption, while pores that are too large allow the suspension to pass through without proper material interaction. Future studies could focus on applying liquid onto scaffolds at different rates and using different suspension buffers to modulate the scaffold imbibition rates to evaluate the impact absorption rate has within the context of a single material.

We did not observe a consistent impact of scaffold absorption dynamics on transduction enhancement. Among successful enhancers, alginate and gelatin maintained the majority of their macrostructure with minimal constriction while hyaluronan and ELP-1 completely dissolved into the droplet during the transduction process. Among poor performers, acrylamide dramatically constricted and strataprene did not change at all during the transduction process. Among intermediate transduction enhancers, 2% agarose minimally constricted while 1% agarose, 1% chitosan, and ELPs-2–4, all ranged from 30% constriction to completely dissolving. These results suggest that the dynamic response of scaffolds to the liquid during the absorption process are neither predictive nor indicative of successful transduction. Rather, these differing responses may be the secondary result of differing solubility, crosslinking, hydrophobicity, charge, and polymer conformational freedom that more directly impact transduction. The initial macrostructure and porous microstructure are important as highlighted by different results from different surface porosities. However, the timescale on which maintaining these structures is critical during transduction is wholly unclear. Future studies could attempt to understand the timescale at which the macrostructure and microstructure impact transduction.

Our data also reveal certain outliers that bucked general trends. For instance, acrylamide scaffolds demonstrated the highest absorption rates and had both surface and bulk porosity, yet they dramatically failed to promote transduction. Although this failure may be attributed to poor cell viability in the acrylamide scaffolds, blended alginate/acrylamide scaffolds retained high cell viability with the same absorption and porosity characteristics to acrylamide and yet did not enhance transduction. On the other hand, ELPs-1–4 had limited surface porosity in the form of fiber-like networks, had high absorption rates and were among the better-performing transduction enhancing materials. Within the materials that had both favorable distributed surface porosity and high absorption rate there are highly differential transduction promoting capacities ranging from ~40% to ~80%, indicating other material characteristics are contributing to this effect.

Our results for the first time also suggest a role for material charge in Drydux-mediated transduction. Charge has been a critical parameter in biomaterials science in a variety of tissue engineering and immunomodulating contexts both *in vitro* and *in vivo*.[49–52] In the case of the saccharides and proteins, negatively charged materials—carboxyl-rich alginate and hyaluronan along with glutamic acid-rich gelatins—resulted in the highest transduction enhancement relative to the no scaffold group. Neutral materials within these groups were the worst performing while positive materials (chitosan) promoted higher levels of transduction. Material charge may be creating electrostatic forces between the scaffold and the cells and viruses in suspension, increasing the likelihood of cell and virus collisions in the scaffold. Alternatively, rather than playing a direct role, charge might impact porosity or liquid absorption, thereby influencing transduction indirectly. Charge, however, is insufficient to fully explain this effect as demonstrated by the ELP constructs. The neutral constructs (ELP-1 and ELP-5) were the best and worst performing constructs, respectively, while the charged constructs (ELPs-2–4) had intermediate levels of transduction enhancement. This suggests a context-dependent role for charge. In the ELP context, dissolution and dynamic rearrangement may take precedent in promoting transduction. Future studies could directly assess the impact of charge through the use of chemically modified materials.[49]

A significant surprise to us was the failure of synthetic materials to enhance transduction. In the case of polyurethane, these scaffolds likely failed because they did not absorb the cell and virus suspension. Absorption into the scaffold and interactions with the material are critically necessary for transduction enhancement. Strataprene, on the other hand, had similar porosity and imbibition rates to other successful materials but failed to enhance transduction. This result again highlights the complex, dynamic nature of the DryDux effect. Strataprene's failure might be attributable to the neutral polymer chain in conjunction with the covalently crosslinked network. Although acrylamide also failed to enhance transduction, this initially was attributed to low cell viability within the scaffold. However, scaffolds made from an interpenetrating network of alginate and acrylamide failed to enhance transduction despite acceptable cell viabilities. The failure of this blend highlights that transduction enhancement is not necessarily an additive characteristic

but rather arises from the complex interplay of the scaffold's material properties.

Overall, we do not have a satisfactory answer to fully explain the Drydux effect but do suggest some guidelines. Complete absorption of the cell and virus suspension into the scaffold is critical. Failure to absorb will result in a failure to enhance transduction. Additionally, on balance, negatively charged polymers outperform neutral or positively charged polymers. Scaffolds with ionic or physical crosslinks outperform covalently crosslinked systems, suggesting a role for polymer strands interacting through dissolution effects.

This report highlights that a variety of materials with differential transduction enhancement capabilities and physical properties are available—enabling selection and derivatization of materials to specific applications. Notably, alginate, gelatin, and hyaluronan scaffolds are straightforward to produce, facilitate high levels of transduction, and have established histories of clinical use, potentially leading to greater commercial viability. Alternatively, materials such as ELPs enable bottom-up design and customization to be tailored to the desired application. These materials provide a foundation from which other materials can be developed, derivatized, and explored to meet pressing needs in the clinic.

In conclusion, the results above clearly define the importance of a holistic materials assessment for design of efficient transduction-promoting reagents and lay the groundwork for further materials improvements. Transduction enhancement is a material-specific phenomenon that is impacted by an interplay of characteristics such as porosity, absorption rate, polymer flexibility, and material charge. Expanding this transduction enhancement phenomenon to scaffolds of diverse materials provides a broader set of tools to streamline cellular therapy manufacturing as well as create innovative systems to meet clinical needs in cellular therapies and regenerative medicine.

Data availability

All raw data from this project are available from the corresponding author upon reasonable request. Supplementary videos can be found at https://doi.org/10.15139/S3/DVGAIU, All data upon which conclusions made from this article are contained within this reports figures and ESI.†

Conflicts of interest

The authors declare the following financial interests/personal relationships which may be considered as potential competing interests: Y. B. and M. M. have pending patents related to CAR T cell production and therapy pending to NC State. Y. B. is the scientific founder of Persistence Therapeutics which seeks to translate technology related to this work. Y. B. has licensed technology for reagents to transduce cells. A. B. is the scientific co-founder of Selsym Biotechnology, which seeks to translate technology unrelated to this work.

Acknowledgements

This work was funded by grants R33CA281875, R21CA277018, and R01EB019409 from the National Institutes of Health, Y20MTS0723 from the UNC Lineberger Comprehensive Cancer Center, the NC State Laboratory Equipment Research Program, and the NC State Comparative Medicine Institute M. M. acknowledges fellowship funding from T32GM141887. S. P. and J. T. M. acknowledges funding from an NSF GFRP Fellowship. This work was performed in part at the Analytical Instrumentation Facility (AIF) at North Carolina State University, which is supported by the State of North Carolina and the National Science Foundation (award number ECCS-2025064). The AIF is a member of the North Carolina Research Triangle Nanotechnology Network (RTNN), a site in the National Nanotechnology Coordinated Infrastructure (NNCI). We thank Chuck Mooney for training and support on the Hitachi SU3900 in the AIF. Flow Cytometry experiments were performed in the Flow Cytometry and Cell Sorting facility at North Carolina State University-College of Veterinary Medicine. We thank Dr David Rose and Dr Lunden Simpson for training and support on the Cytoflex in the flow cytometry core. We acknowledge the NC State library for providing access to Fujifilm cameras for photography and video.

References

1 D. Han, Z. Xu, Y. Zhuang, Z. Ye and Q. Qian, Current Progress in CAR-T Cell Therapy for Hematological Malignancies, *J. Cancer*, 2021, **12**(2), 326–334, DOI: **10.7150/jca.48976**.

2 X. Zhang, L. Zhu, H. Zhang, S. Chen and Y. Xiao, CAR-T Cell Therapy in Hematological Malignancies: Current Opportunities and Challenges, *Front. Immunol.*, 2022, **13**, 927153, DOI: **10.3389/fimmu.2022.927153**.

3 R. A. Attia, G. S. A. Qureshi, M. Safdar, A. Raafat, G. Janardhan, H. A. H. Elshamy and J. Malay, Gene Therapy: A Revolutionary Step in Treating Thalassemia, *Preprints*, 2024. DOI: **10.20944/preprints202406.0024.v1**.

4 D. V. Parums, Editorial: First Regulatory Approvals for CRISPR-Cas9 Therapeutic Gene Editing for Sickle Cell Disease and Transfusion-Dependent β-Thalassemia, *Med. Sci. Monit.*, 2024, **30**, e944204, DOI: **10.12659/MSM.944204**.

5 J.-A. Ribeil, S. Hacein-Bey-Abina, E. Payen, A. Magnani, M. Semeraro, E. Magrin, L. Caccavelli, B. Neven, P. Bourget, W. El Nemer, P. Bartolucci, L. Weber, H. Puy, J.-F. Meritet, D. Grevent, Y. Beuzard, S. Chrétien, T. Lefebvre, R. W. Ross, O. Negre, G. Veres, L. Sandler, S. Soni, M. de Montalembert, S. Blanche, P. Leboulch and M. Cavazzana, Gene Therapy in a Patient with Sickle Cell Disease, *N. Engl. J. Med.*, 2017, **376**(9), 848–855, DOI: **10.1056/NEJMoa1609677**.

6 S. Tyagarajan, T. Spencer and J. Smith, Optimizing CAR-T Cell Manufacturing Processes during Pivotal Clinical Trials,

Mol. Ther.-Methods Clin. Dev., 2020, **16**, 136–144, DOI: **10.1016/j.omtm.2019.11.018**.

7 M. Poorebrahim, S. Sadeghi, E. Fakhr, M. F. Abazari, V. Poortahmasebi, A. Kheirollahi, H. Askari, A. Rajabzadeh, M. Rastegarpanah, A. Linē and A. Cid-Arregui, Production of CAR T-Cells by GMP-Grade Lentiviral Vectors: Latest Advances and Future Prospects, *Crit. Rev. Clin. Lab. Sci.*, 2019, **56**(6), 393–419, DOI: **10.1080/10408363.2019.1633512**.

8 P. Agarwalla, E. A. Ogunnaike, S. Ahn, F. S. Ligler, G. Dotti and Y. Brudno, Scaffold-Mediated Static Transduction of T Cells for CAR-T Cell Therapy, *Adv. Healthcare Mater.*, 2020, **9**(14), e2000275, DOI: **10.1002/adhm.202000275**.

9 M. VanBlunk, V. Srikanth, S. S. Pandit, A. V. Kuznetsov and Y. Brudno, Absorption Rate Governs Cell Transduction in Dry Macroporous Scaffolds, *Biomater. Sci.*, 2023, **11**(7), 2372–2382, DOI: **10.1039/d2bm01753a**.

10 M. VanBlunk, P. Agarwalla, S. Pandit and Y. Brudno, Fabrication and Use of Dry Macroporous Alginate Scaffolds for Viral Transduction of T Cells, *J. Visualized Exp.*, 2022, (187), e64036, DOI: **10.3791/64036**.

11 S. Pandit, P. Agarwalla, F. Song, A. Jansson, G. Dotti and Y. Brudno, Implantable CAR T Cell Factories Enhance Solid Tumor Treatment, *Biomaterials*, 2024, **308**(122580), 122580, DOI: **10.1016/j.biomaterials.2024.122580**.

12 P. Agarwalla, E. A. Ogunnaike, S. Ahn, K. A. Froehlich, A. Jansson, F. S. Ligler, G. Dotti and Y. Brudno, Bioinstructive Implantable Scaffolds for Rapid in Vivo Manufacture and Release of CAR-T Cells, *Nat. Biotechnol.*, 2022, **40**(8), 1250–1258, DOI: **10.1038/s41587-022-01245-x**.

13 S. Saha, S. Banskota, J. Liu, N. Zakharov, M. Dzuricky, X. Li, P. Fan, S. Deshpande, I. Spasojevic, K. Sharma, M. J. Borgnia, J. L. Schaal, A. Raman, S. Kim, J. Bhattacharyya and A. Chilkoti, Genetically Engineered Nanoparticles of Asymmetric Triblock Polypeptide with a Platinum(IV) Cargo Outperforms a Platinum(II) Analog and Free Drug in a Murine Cancer Model, *Nano Lett.*, 2022, **22**(14), 5898–5908, DOI: **10.1021/ACS.NANOLETT.2C01850/ASSET/IMAGES/LARGE/NL2C01850_0005.JPEG**.

14 S. Saha, S. Banskota, S. Roberts, N. Kirmani and A. Chilkoti, Engineering the Architecture of Elastin–Like Polypeptides: From Unimers to Hierarchical Self–Assembly, *Adv. Ther.*, 2020, **3**(3), 1900164, DOI: **10.1002/adtp.201900164**.

15 S. Roberts, T. S. Harmon, J. L. Schaal, V. Miao, K. (jonathan) Li, A. Hunt, Y. Wen, T. G. Oas, J. H. Collier, R. V. Pappu and A. Chilkoti, Injectable Tissue Integrating Networks from Recombinant Polypeptides with Tunable Order, *Nat. Mater.*, 2018, **17**(12), 1154–1163, DOI: **10.1038/s41563-018-0182-6**.

16 P. Patil, K. A. Russo, J. T. McCune, A. C. Pollins, M. A. Cottam, B. R. Dollinger, C. R. DeJulius, M. K. Gupta, R. D'Arcy, J. M. Colazo, F. Yu, M. G. Bezold, J. R. Martin, N. L. Cardwell, J. M. Davidson, C. M. Thompson, A. Barbul, A. H. Hasty, S. A. Guelcher and C. L. Duvall, Reactive Oxygen Species-Degradable Polythioketal Urethane Foam Dressings to Promote Porcine Skin Wound Repair, *Sci. Transl. Med.*, 2022, **14**(641), eabm6586, DOI: **10.1126/scitranslmed.abm6586**.

17 W. L. Murphy, R. G. Dennis, J. L. Kileny and D. J. Mooney, Salt Fusion: An Approach to Improve Pore Interconnectivity within Tissue Engineering Scaffolds, *Tissue Eng.*, 2002, **8**(1), 43–52, DOI: **10.1089/107632702753503045**.

18 A. Biomatrix, SpongeCol: Product Description. **https://advancedbiomatrix.com/spongecol.html**.

19 K. Y. Lee and D. J. Mooney, Alginate: Properties and Biomedical Applications, *Prog. Polym. Sci.*, 2012, **37**(1), 106–126, DOI: **10.1016/j.progpolymsci.2011.06.003**.

20 Y. Brudno, M. J. Pezone, T. K. Snyder, O. Uzun, C. T. Moody, M. Aizenberg and D. J. Mooney, Replenishable Drug Depot to Combat Post-Resection Cancer Recurrence, *Biomaterials*, 2018, **178**, 373–382, DOI: **10.1016/j.biomaterials.2018.05.005**.

21 C. T. Moody, S. Palvai and Y. Brudno, Click Cross-Linking Improves Retention and Targeting of Refillable Alginate Depots, *Acta Biomater.*, 2020, **112**, 112–121, DOI: **10.1016/j.actbio.2020.05.033**.

22 A. Yasin, Y. Ren, J. Li, Y. Sheng, C. Cao and K. Zhang, Advances in Hyaluronic Acid for Biomedical Applications, *Front. Bioeng. Biotechnol.*, 2022, **10**, 910290, DOI: **10.3389/fbioe.2022.910290**.

23 M. Dovedytis, Z. J. Liu and S. Bartlett, Hyaluronic Acid and Its Biomedical Applications: A Review, *Eng. Regener.*, 2020, **1**, 102–113, DOI: **10.1016/j.engreg.2020.10.001**.

24 G. D. Prestwich, Hyaluronic Acid-Based Clinical Biomaterials Derived for Cell and Molecule Delivery in Regenerative Medicine, *J. Controlled Release*, 2011, **155**(2), 193–199, DOI: **10.1016/j.jconrel.2011.04.007**.

25 F. S. Rezaei, F. Sharifianjazi, A. Esmaeilkhanian and E. Salehi, Chitosan Films and Scaffolds for Regenerative Medicine Applications: A Review, *Carbohydr. Polym.*, 2021, **273**(118631), 118631, DOI: **10.1016/j.carbpol.2021.118631**.

26 M. Rodríguez-Vázquez, B. Vega-Ruiz, R. Ramos-Zúñiga, D. A. Saldaña-Koppel and L. F. Quiñones-Olvera, Chitosan and Its Potential Use as a Scaffold for Tissue Engineering in Regenerative Medicine, *BioMed Res. Int.*, 2015, **2015**, 1–15, DOI: **10.1155/2015/821279**.

27 B. P. Koppolu, S. G. Smith, S. Ravindranathan, S. Jayanthi, T. K. Suresh Kumar and D. A. Zaharoff, Controlling Chitosan-Based Encapsulation for Protein and Vaccine Delivery, *Biomaterials*, 2014, **35**(14), 4382–4389, DOI: **10.1016/j.biomaterials.2014.01.078**.

28 D. A. Zaharoff, C. J. Rogers, K. W. Hance, J. Schlom and J. W. Greiner, Chitosan Solution Enhances Both Humoral and Cell-Mediated Immune Responses to Subcutaneous Vaccination, *Vaccine*, 2007, **25**(11), 2085–2094, DOI: **10.1016/j.vaccine.2006.11.034**.

29 F. Jiang, X.-W. Xu, F.-Q. Chen, H.-F. Weng, J. Chen, Y. Ru, Q. Xiao and A.-F. Xiao, Extraction, Modification and Biomedical Application of Agarose Hydrogels: A Review, *Mar. Drugs*, 2023, **21**(5), 299, DOI: **10.3390/md21050299**.

30 B. Niemczyk-Soczynska, D. Kolbuk, G. Mikulowski, I. A. Ciechomska and P. Sajkiewicz, Methylcellulose/Agarose Hydrogel Loaded with Short Electrospun PLLA/Laminin Fibers as an Injectable Scaffold for Tissue Engineering/3D Cell Culture Model for Tumour Therapies, *RSC Adv.*, 2023, **13**(18), 11889–11902, DOI: **10.1039/d3ra00851g**.

31 E. Varoni, M. Tschon, B. Palazzo, P. Nitti, L. Martini and L. Rimondini, Agarose Gel as Biomaterial or Scaffold for Implantation Surgery: Characterization, Histological and Histomorphometric Study on Soft Tissue Response, *Connect. Tissue Res.*, 2012, **53**(6), 548–554, DOI: **10.3109/03008207.2012.712583**.

32 P. Sukhavattanakul, P. Pisitsak, S. Ummartyotin and R. Narain, Polysaccharides for Medical Technology: Properties and Applications, *Macromol. Biosci.*, 2023, **23**(2), e2200372, DOI: **10.1002/mabi.202200372**.

33 E. Rezvani Ghomi, N. Nourbakhsh, M. Akbari Kenari, M. Zare and S. Ramakrishna, Collagen–based Biomaterials for Biomedical Applications, *J. Biomed. Mater. Res.*, 2021, **109**(12), 1986–1999, DOI: **10.1002/jbm.b.34881**.

34 E. J. Sheehy, G. M. Cunniffe and F. J. O'Brien, Collagen-Based Biomaterials for Tissue Regeneration and Repair, in *Peptides and Proteins as Biomaterials for Tissue Regeneration and Repair*, ed. M. A. Barbosa and M. C. L. Martins, Elsevier, 2018, pp. 127–150. DOI: **10.1016/b978-0-08-100803-4.00005-x**.

35 K. Lin, D. Zhang, M. H. Macedo, W. Cui, B. Sarmento and G. Shen, Advanced Collagen–Based Biomaterials for Regenerative Biomedicine, *Adv. Funct. Mater.*, 2019, **29**(3), 1804943, DOI: **10.1002/adfm.201804943**.

36 S. Chattopadhyay and R. T. Raines, Review Collagen-Based Biomaterials for Wound Healing: Collagen-Based Biomaterials, *Biopolymers*, 2014, **101**(8), 821–833, DOI: **10.1002/bip.22486**.

37 Y. Dong, A. Sigen, M. Rodrigues, X. Li, S. H. Kwon, N. Kosaric, S. Khong, Y. Gao, W. Wang and G. C. Gurtner, Injectable and Tunable Gelatin Hydrogels Enhance Stem Cell Retention and Improve Cutaneous Wound Healing, *Adv. Funct. Mater.*, 2017, **27**(24), 1606619, DOI: **10.1002/adfm.201606619**.

38 T. Rajangam and S. S. A. An, Fibrinogen and Fibrin Based Micro and Nano Scaffolds Incorporated with Drugs, Proteins, Cells and Genes for Therapeutic Biomedical Applications, *Int. J. Nanomed.*, 2013, **8**, 3641–3662, DOI: **10.2147/IJN.S43945**.

39 H. Simaan-Yameen, O. Bar-Am, G. Saar and D. Seliktar, Methacrylated Fibrinogen Hydrogels for 3D Cell Culture and Delivery, *Acta Biomater.*, 2023, **164**, 94–110, DOI: **10.1016/j.actbio.2023.03.046**.

40 T. Buie, J. McCune and E. Cosgriff-Hernandez, Gelatin Matrices for Growth Factor Sequestration, *Trends Biotechnol.*, 2020, **38**(5), 546–557, DOI: **10.1016/j.tibtech.2019.12.005**.

41 J. Despanie, J. P. Dhandhukia, S. F. Hamm-Alvarez and J. A. MacKay, Elastin-like Polypeptides: Therapeutic Applications for an Emerging Class of Nanomedicines, *J. Controlled Release*, 2016, **240**, 93–108, DOI: **10.1016/j.jconrel.2015.11.010**.

42 A. Jiang, X. Guan, L. He and X. Guan, Engineered Elastin-like Polypeptides: An Efficient Platform for Enhanced Cancer Treatment, *Front. Pharmacol.*, 2022, **13**, 1113079, DOI: **10.3389/fphar.2022.1113079**.

43 G. Sennakesavan, M. Mostakhdemin, L. K. Dkhar, A. Seyfoddin and S. J. Fatihhi, Acrylic Acid/Acrylamide Based Hydrogels and Its Properties - A Review, *Polym. Degrad. Stab.*, 2020, **180**(109308), 109308, DOI: **10.1016/j.polymdegradstab.2020.109308**.

44 S. Van Vlierberghe, P. Dubruel and E. Schacht, Biopolymer-Based Hydrogels as Scaffolds for Tissue Engineering Applications: A Review, *Biomacromolecules*, 2011, **12**(5), 1387–1408, DOI: **10.1021/bm200083n**.

45 Z. Terzopoulou, A. Zamboulis, I. Koumentakou, G. Michailidou, M. J. Noordam and D. N. Bikiaris, Biocompatible Synthetic Polymers for Tissue Engineering Purposes, *Biomacromolecules*, 2022, **23**(5), 1841–1863, DOI: **10.1021/acs.biomac.2c00047**.

46 P. Gunatillake and R. Adhikari, Biodegradable Synthetic Polymers for Tissue Engineering, *Eur. Cells Mater.*, 2003, **5**, 1–16, DOI: **10.22203/ECM.V005A01**, discussion16.

47 D. Wienen, T. Gries, S. L. Cooper and D. E. Heath, An Overview of Polyurethane Biomaterials and Their Use in Drug Delivery, *J. Controlled Release*, 2023, **363**, 376–388, DOI: **10.1016/j.jconrel.2023.09.036**.

48 C. E. Nelson, A. J. Kim, E. J. Adolph, M. K. Gupta, F. Yu, K. M. Hocking, J. M. Davidson, S. A. Guelcher and C. L. Duvall, Tunable Delivery of SiRNA from a Biodegradable Scaffold to Promote Angiogenesis in Vivo, *Adv. Mater.*, 2014, **26**(4), 607–614, DOI: **10.1002/adma.201303520**.

49 A. Schulz, A. Katsen-Globa, E. J. Huber, S. C. Mueller, A. Kreiner, N. Pütz, M. M. Gepp, B. Fischer, F. Stracke, H. von Briesen, J. C. Neubauer and H. Zimmermann, Poly (Amidoamine)-Alginate Hydrogels: Directing the Behavior of Mesenchymal Stem Cells with Charged Hydrogel Surfaces, *J. Mater. Sci. Mater. Med.*, 2018, **29**(7), 105, DOI: **10.1007/s10856-018-6113-x**.

50 M. Rahmati, E. A. Silva, J. E. Reseland, C. A. Heyward and H. J. Haugen, Biological Responses to Physicochemical Properties of Biomaterial Surface, *Chem. Soc. Rev.*, 2020, **49**(15), 5178–5224, DOI: **10.1039/d0cs00103a**.

51 H. Amani, H. Arzaghi, M. Bayandori, A. S. Dezfuli, H. Pazoki-Toroudi, A. Shafiee and L. Moradi, Controlling Cell Behavior through the Design of Biomaterial Surfaces: A Focus on Surface Modification Techniques, *Adv. Mater. Interfaces*, 2019, **6**(13), 1900572, DOI: **10.1002/admi.201900572**.

52 S. Metwally and U. Stachewicz, Surface Potential and Charges Impact on Cell Responses on Biomaterials Interfaces for Medical Applications, *Mater. Sci. Eng., C*, 2019, **104**(109883), 109883, DOI: **10.1016/j.msec.2019.109883.**.